Polarized absorption and anomalous temperature dependence of fluorescence depolarization in cylindrical J-aggregates

Spitz, C.; Knoester, J.; Ouart, A.; Daehne, S.

Published in:
Chemical Physics

DOI:
10.1016/S0301-0104(01)00521-3

Publication date:
2002

ELSEVIER

Chemical Physics 275 (2002) 271–284

Chemical Physics

www.elsevier.com/locate/chemphys

Polarized absorption and anomalous temperature dependence of fluorescence depolarization in cylindrical *J*-aggregates

Christian Spitz[a,d], Jasper Knoester[b], André Ouart[c], Siegfried Daehne[a,*]

[a] *Federal Institute for Materials Research and Testing, Richard-Willstaetter-Strasse 11, D-12489 Berlin, Germany*
[b] *Institute for Theoretical Physics and Materials Science Center, University of Groningen, Nijenborgh 4, 9747 AG Groningen, The Netherlands*
[c] *Institute of Chemistry, Humboldt University, Hessische Strasse 1-2, D-10115 Berlin, Germany*
[d] *Institute of Physics, University of Potsdam, Am Neuen Palais 10, D-14415 Potsdam, Germany*

Received 11 April 2001; in final form 4 July 2001

Abstract

We study chiral *J*-aggregates of the amphiphilic dye **1A** that are spontaneously and asymmetrically generated from achiral dye monomers. These aggregates occur in two types. One type possesses a threefold split *J*-absorption band and forms micrometer-sized superhelices. The other type has a twofold split *J*-absorption band and forms smaller nanoparticles. We show that the analysis of optical experiments with polarized light in terms of an exciton model yields strong indications that the smaller aggregates have a cylindrical structure as well; the lower exciton band is polarized along the cylinder axis, while the higher band is polarized perpendicular to it. Our analysis allows for an estimate of the number of molecules around the circumference of the cylinder. Fluorescence–polarization excitation spectra at room temperature confirm the cylinder model. At low temperature, these spectra reveal a surprising loss of fluorescence polarization upon excitation in the higher exciton band. Possible explanations for this observation are discussed.

1. Introduction

The light-harvesting complexes (LHCs) of photosynthetic bacteria and plants consist of strongly coupled and highly ordered assemblies of chlorophyll molecules and their derivatives which absorb light energy and transfer it through many dye molecules in direction to the photosynthetic reaction center [1–3]. Especially the very efficient LHC LH2 of purple bacteria adopts a tight ring-shaped structure with a diameter of 7 nm which is built up from 16 or 18 bacteriochlorophyll a (Bchl-a) molecules. The absorbed light energy is then transferred to the LHC LH1, where it triggers photosynthesis in the reaction center. Also the LH1 complex has a ring structure containing 32 Bchl-a molecules. The nature of the exciton states in LH2 has been the topic of many recent studies.

* Corresponding author. Fax: +30-8104-1137.
E-mail address: siegfried.daehne@bam.de (S. Daehne).

0301-0104/02/$ - see front matter
PII: S0301-0104(01)00521-3

In particular the extent of the exciton wave function (the delocalization length) is a source of much debate [4]. Strong indications exist that, at least at low temperature, the initially excited states in the B850 ring are coherently delocalized over a major part of the ring [5].

In order to mimic LHCs it will be necessary to develop supramolecular dye assemblies which have giant absorption cross-section and the ability of fast and efficient excitation energy migration. Such assemblies are the well-known *J*-aggregates of organic dyes [6,7]. They are further characterized by resonance fluorescence of high quantum yield and by absorption bands in the visible region that are exchange-narrowed and red-shifted relative to the broad absorption band of the monomeric molecules [8–11]. However, in order to realize cyclic *J*-aggregates similar to the natural LHCs, it was necessary to develop a new type of dyes **1** [$R = C_nH_{2n+1}$; $R' = (CH_2)_m$–X with $n > 6$, $m = 2$ or 3, X = SO_3H or COOH], whose molecules are amphiphilic in nature and contain both hydrophobic alkyl groups and hydrophilic acidic substituents [12–14]. In aqueous solution such dyes form *J*-aggregates that show the effect of pigment interaction performing energy-migration (PIPE) effect. Consequently, the *J*-aggregates of the amphiphilic dyes are designated amphi-PIPEs (cf. Scheme 1). Depending on the substituents of the aggregating dyes as well as on the environment, the amphi-PIPEs exist either as ribbons [15], nanotubes [16], vesicles [16], or even as spontaneously and enantioselectively generated chiral entities like superhelices [15,17].

In this paper we study the linear spectroscopy of chiral *J*-aggregates generated from the achiral dye **1A** (**1**, $R = C_8H_{17}$; $R' = (CH_2)_3$ COOH).

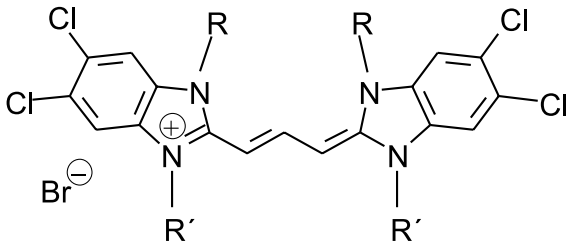

Scheme 1. Dye **1**.

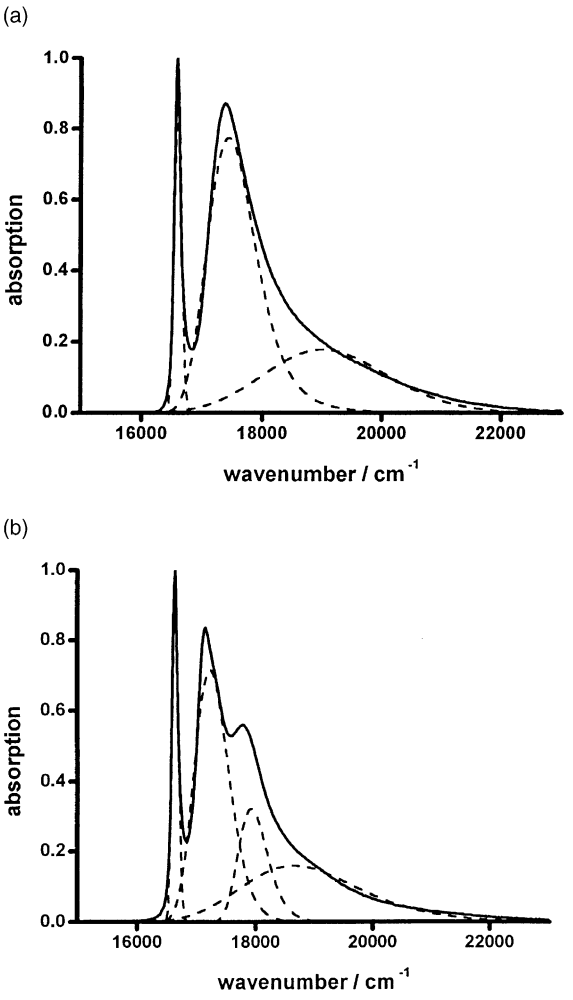

Fig. 1. Absorption spectra in the visible region of dye **1A** *J*-aggregates having a twofold split (a) and a threefold split (b) *J*-band (—) and their constituent single peaks after deconvolution by asymmetrical Gaussian functions (- - -). (a) 1.0 ml 10^{-4} mol l^{-1} dye solution in methanol plus 9.0 ml 10^{-2} mol l^{-1} aqueous sodium hydroxide solution in 1 cm cuvette. The single peaks are positioned at 16 592 cm^{-1} [82.3 cm^{-1}; 9.59], 17 422 cm^{-1} [556.9 cm^{-1}; 54.93], and 19 000 cm^{-1} [1436.9 cm^{-1}; 25.21]. The values in brackets are the FWHM and the relative areas of the peaks. The correlation coefficient of goodness of deconvolution is $R^2 = 0.9888$. (b) 5.8×10^{-7} mol l^{-1} dye directly solved in 20 ml 10^{-2} mol l^{-1} aqueous sodium hydroxide solution, thickness of the cuvette 1 cm. The single peaks are positioned at 16 636 cm^{-1} [79.5 cm^{-1}; 9.53], 17 199 cm^{-1} [371.5 cm^{-1}; 32.52], 17 861 cm^{-1} [351.0 cm^{-1}; 17.33] and 19 000 cm^{-1} [1436.9 cm^{-1}; 22.65]. The values in brackets are the FWHM and the relative areas of the peaks. The correlation coefficient of goodness of deconvolution is $R^2 = 0.9837$.

From their spectral behavior it turns out that these aggregates exist in two different species (cf. Fig. 1). One type has a threefold split *J*-absorption band with maxima at 562, 583, and 600 nm. According to cryogenic transmission electron microscopy (cryo-TEM) this type forms micrometer-sized, rope-like superhelices consisting of several cylindrical strands that have a diameter of about 10 nm each [15]. Presumably, the cylinders are composed of bilayers similar to the other amphi-PIPEs consisting of the same chromophore [14]. In this case the octyl groups of the coupled dye molecules interact with each other by hydrophobical forces in order to ensure the bilayer structure, whereas the acidic carboxypropyl substituents of the inner layer point to the center of the cylinder and that of the outer layer interact with the water molecules of the solvent used. The superhelices can be separated from solution by filtration through nylon filters having pores of 0.22 μm diameter (cf. Section 3). Owing to their μm size scale, they exhibit strong light scattering effects, which, unfortunately, prevent polarization dependent measurements.

The other type of *J*-aggregates, which will be the main focus of this work, has a twofold split *J*-absorption band with maxima at 576 and 606 nm. These aggregates must be very small, because they pass the above mentioned nylon filter, exhibit less light scattering and, hitherto, it was not possible to visualize them by cryo-TEM. Therefore, it is supposed that these *J*-aggregates have a micellar structure consisting of coupled dye molecules whose octyl groups point to the center of the micelle forming there a quasi-liquid phase, whereas the acidic carboxypropyl groups are at the surface of the micelle [14]. As the small *J*-aggregates are optically active, just like the larger ones, the basic question to be answered is whether the small aggregates also have a cyclic or even a cylindrical structure, similar to the single strands of the superhelices. From recent measurements of the absorption and fluorescence spectra under high pressure, it was concluded already that the small *J*-aggregates should have a hollow structure [18].

In this paper we briefly present some of the essential elements of the theory of the spectral behavior of cylindrical *J*-aggregates (Section 2), we explore the experimental conditions to prepare different, optically active *J*-aggregates of dye **1A** (Section 3), and we determine the polarization of the transition moments relative to the *J*-aggregates' axes and investigate the fluorescence polarization of the small *J*-aggregates in dependence on temperature (Section 4). The results strongly support the assumption that the small *J*-aggregates possess a cylindrical architecture as well. We conclude in Section 5.

2. Theory of spectral behavior of cylindrical *J*-aggregates

In order to model the spectral behavior of cylindrical *J*-aggregates we assume that they are built up from weakly interacting rings, each containing N_{ring} identical molecules which are inclined by the angle β with respect to the ring's plane, as shown in Fig. 2. Each ring is chiral and displays optical activity provided that $\beta \neq 0°$, $\neq 90°$, and $\neq 180°$. One enantiomer has angles β between 0° and 90°, the other one between 90° and 180°. It is assumed that the single strands of the large superhelices also consist of such rings that are stacked up to cylinders [15,19]. As can be seen in Fig. 2, by the stacking procedure in each cylinder N_{ring} intertwined single helices are formed which might enhance the observed optical activity.

As is appropriate for molecular systems, we will use the Frenkel exciton model to describe the excited states [20]. Since we do not have detailed knowledge of the aggregate structure, we will take the simplest point of view and restrict ourselves to nearest neighbor excitation transfer interactions J between the molecules within each ring; interactions between rings are assumed to be sufficiently weak to be ignored. A more detailed treatment, dealing with long-range interactions both inside rings and between molecules in different rings is presented in Ref. [21]. Such an extension does not affect the essential properties to be described below (notably the existence of two linear optical transitions with perpendicular polarization), but it does affect the parameters that can be deduced from comparison to experiment (also see Section 5). In the subspace of singly excited states, which are the

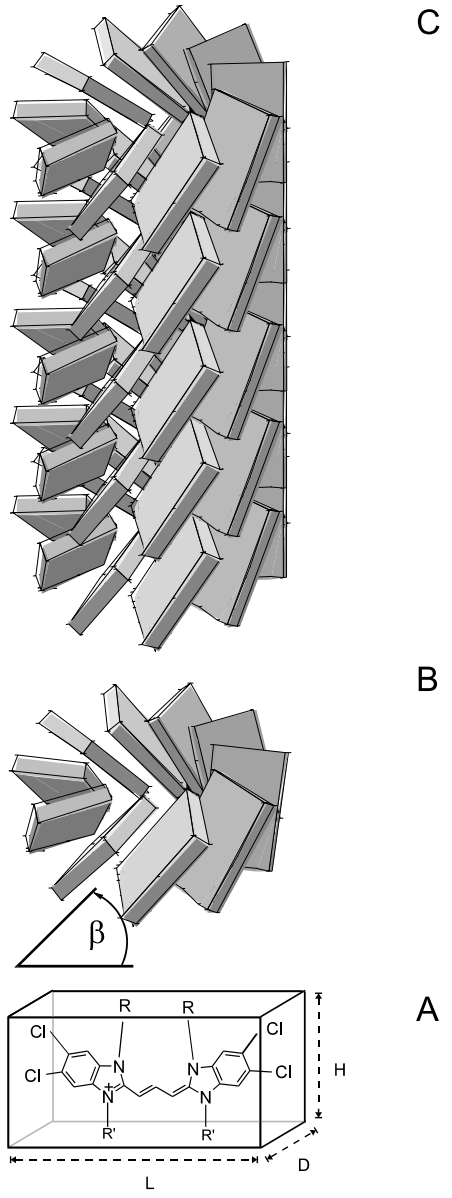

Fig. 2. Demonstration of circular arrangement of the molecules in the J-aggregate: (a) each dye molecule is represented by a box with the dimensions $L = 1.9$ nm, $H = 1.0$ nm, and $D = 0.4$ nm. The octyl substituents R are taken outside of the box. The transition dipole moment $\vec{\mu}_n^0$ lies in direction of the long edge of the box. (b) In this example a circle is built by $N_{\text{ring}} = 10$ molecules which are tilted by angle β in respect to the circle plane. The thickness D of the molecules is taken equal to the distance between the axes of neighbored molecules. (c) A cylinder consisting of a tenfold helix which is formed by putting five rings one upon another.

only ones of interest to linear optics, the relevant Hamiltonian for a single ring reads:

$$H = \sum_{n=1}^{N_{\text{ring}}} E^0 |n\rangle\langle n| + J(|n\rangle\langle n+1| + |n+1\rangle\langle n|). \quad (1)$$

Here, $|n\rangle$ is the state with molecule n in its excited state and all other molecules in their ground states, E^0 is the excitation energy of an isolated molecule and disorder is neglected. From the diagonalization of this Hamiltonian one obtains its eigenvalues E_k and eigenvectors $\boldsymbol{a}_k = (a_{k,1}, \ldots, a_{k.N})$ which determine the energy eigenstates of the aggregate:

$$|\Psi_k\rangle = \sum_n a_{k,n} |n\rangle. \quad (2)$$

As cyclic boundary conditions naturally apply for a single ring, the eigenstates are the Bloch functions

$$|\Psi_k\rangle = \sqrt{\frac{1}{N_{\text{ring}}}} \sum_n \mathrm{e}^{2\pi \mathrm{i} k (n/N_{\text{ring}})} |n\rangle$$
$$(k = 0, \pm 1, \pm 2, \ldots, N_{\text{ring}}/2) \quad (3)$$

with energies split into the exciton band

$$E_k = E^0 + 2J \cos\left(\frac{2\pi k}{N_{\text{ring}}}\right). \quad (4)$$

It is obvious that for J-aggregates, i.e., aggregates with $J < 0$, the $k = 0$ state represents the lower edge of the exciton band.

Because the transition dipole moments of the exciton states $\vec{\mu}_k$ result from summing over the transition dipole moments of the individual molecules $\vec{\mu}_n^0$ weighted by the amplitude of the molecule n in the wave function,

$$\vec{\mu}_k = \sum_n a_k \vec{\mu}_k^0 = \sqrt{\frac{1}{N_{\text{ring}}}} \sum \mathrm{e}^{2\pi \mathrm{i} k (n/N_{\text{ring}})} \vec{\mu}_n^0 \quad (5)$$

the optical interaction of the exciton states depends on the direction of the transition dipoles of the individual molecules in the aggregate. For instance, it is well known that in linear chains, with all molecules having the same orientation, only $\vec{\mu}_{k=0}$ differs from zero. Therefore, linear J-aggregates consisting of N molecules exhibit only one absorption line, corresponding to the lowest exciton transition and having an oscillator

strength that is enhanced by a factor of N compared to the individual molecules.

A different situation arises in circular aggregates [22]. Let us assume that the molecules form a ring in x–y plane, with dipoles along the long molecular axes (cf. Fig. 2). Then, on the one hand for the $k = 0$ state only the z-components of the $\vec{\mu}_n^0$ sum up constructively, while the in-plane components compensate to yield exactly zero. On the other hand for the two degenerate states with $k = \pm 1$ the in-plane components of $\vec{\mu}_n^0$ sum up constructively, giving rise to a finite oscillator strength of these states, while the z-components compensate to zero. The transitions to all other Bloch states have vanishing oscillator strength. Therefore, a circular J-aggregate with molecular transition dipole moments that are neither exactly in the plane of the ring nor exactly perpendicular to it, reveals an absorption spectrum with two absorption bands. The transition to the lower lying $k = 0$ state is polarized perpendicular to the circle plane (i.e., along our cylinder axis), while the transitions to the higher lying $k = \pm 1$ states are polarized in the plane of the ring (perpendicular to the cylinder axis).

It is of interest to note that measurement of the positions of these two exciton absorption lines, together with knowledge of the monomer transition energy, suffices to obtain the number of molecules in the ring N_{ring} according to:

$$\cos\left(\frac{2\pi}{N_{\text{ring}}}\right) = \frac{E_{k=\pm1} - E^0}{E_{k=0} - E^0}. \tag{6}$$

Thus, N_{ring} determines the splitting between the two lines resulting from $k = 0$ and $k = \pm 1$. This even holds in the presence of long-range interactions inside a particular ring or between molecules residing on two distinct rings [21]. Then, however, one needs detailed knowledge of these additional interactions in order to extract N_{ring} from the measured spectra.

Obviously, the transition dipoles from the aggregate ground state to the three dipole allowed exciton states depend on the tilt angle β between the transition dipole moments of the molecules and the circle plane (see Fig. 2). Performing the sum in Eq. (5) one obtains:

$$\begin{aligned} \vec{\mu}_0 &= \sqrt{N_{\text{ring}}}\vec{e}_z \sin(\beta)\mu^0, \\ \vec{\mu}_{\pm1} &= \tfrac{1}{2}\sqrt{N_{\text{ring}}}(\vec{e}_x \mp \mathrm{i}\vec{e}_y)\cos(\beta)\mu^0, \end{aligned} \tag{7}$$

where μ^0 denotes the magnitude of the molecular transition dipoles. It is now straightforward to relate the ratio of the total intensities $A_{k=0}$ and $A_{k=\pm1}$ (integrated absorption profiles of both lines) to the angle β. Accounting for the degeneracy of the $k = \pm 1$ states, one arrives at

$$\frac{A_{k=0}}{A_{k=\pm1}} = \frac{|\vec{\mu}_0|^2}{(|\vec{\mu}_1|^2 + |\vec{\mu}_{-1}|^2)} = \tan^2(\beta). \tag{8}$$

This gives the interesting possibility to determine the angle β from integrating the two observed absorption lines. Eq. (8) is not altered by inclusion of long-range intra-ring and inter-ring interactions [21].

Of course, in practice both absorption lines are broadened by disorder. As long as the disorder is weak relative to the splitting between the two peaks, the disorder will not strongly mix the nondegenerate Bloch states and the above picture derived for perfectly ordered aggregates, still captures the essential physics, provided that one allows for broadening of the two absorption lines. In this weak-disorder situation, the amount of line broadening is reduced by exchange narrowing [8–11]. For the higher-energy ($k = \pm 1$) absorption line, the narrowing factor is less than for the $k = 0$ state, as a consequence of the disorder-induced splitting within the degenerate pair. In the case of fast dynamic energy disorder, it has been shown that the higher-energy ($k = \pm 1$) line is twice as broad as the low-energy ($k = 0$) one [23], while in the case of static energy disorder, the difference is a factor of $\sqrt{2}$ [24]. Moreover, the higher line is also broadened by energy relaxation to the lower state. Thus, quite generally, the absorption spectrum of a cyclic J-aggregate is expected to exhibit two absorption lines, where the higher-energy one is appreciably broader than the lower-energy one. This provides a natural explanation for the twofold split absorption spectrum in Fig. 1(a). We will come back to this in more detail in Section 4.

In fact, the above model for J-aggregates having a cyclic structure also allows for a plausible interpretation of the threefold split absorption spectrum

(Fig. 1(b)) of the large superhelices of dye **1A**. As already mentioned the diameter of their constituent single strands of about 10 nm is too large for the formation of single-walled micelles. Therefore, it is likely that the single strands are bilayer tubules having a bilayer thickness of 4 ± 0.5 nm [15]. If so, the inner layer must contain fewer molecules than the outer one, provided that the intermolecular distances are the same in both layers. Thus, as the energies of the $k = \pm 1$ states (polarized perpendicular to the cylinder axis) depend on N_{ring}, these transitions have different absorption energies for the inner and outer ring of the bilayer, whereas the $k = 0$ states of both layers (polarized parallel to the axis) have identical energies (assuming the monomer transition energy and the intermolecular interaction to be the same for both layers). This automatically gives rise to a spectrum with three *J*-absorption peaks (cf. Fig. 1(b)).

3. Sample preparation

Dye **1A** used in this paper was purchased from FEW Chemicals [25] and purified by recrystallization from dimethylsulfoxide (DMSO). The molar extinction coefficient of the pure dye in both DMSO and methanol amounts to 185 000 $cm^2\,mmol^{-1}$, having absorption maximum at 528 nm in DMSO and at 523 nm in methanol with halfwidth (FWHM) of the absorption band of 1436 cm^{-1} in DMSO [26]. [1]

To prepare *J*-aggregates with a threefold split absorption spectrum with maxima at 562, 583, and 600 nm (shown in Fig. 1(b)), the crystalline powder of the dye is solved in 10^{-2} mol l^{-1} aqueous sodium hydroxide solution by stirring for 24 h under argon atmosphere [15]. The nylon filters used for separating the *J*-aggregates from solution were purchased from Micron Separations, Inc., Westboro, MA, USA. In order to prepare *J*-aggregates having a twofold split absorption spectrum with maxima at 576 and 606 nm (shown in Fig. 1(a)), either ethanol is added to the solutions with *J*-aggregates having a threefold split absorption spectrum or dye **1A** is first solved in ethanol and this stock solution is then slowly poured into a 10^{-2} mol l^{-1} sodium hydroxide solution.

The regions for the existence of two- and threefold split *J*-aggregates of dye **1A** in dependence on the concentration of the dye and the ethanol content of the solution are given in Fig. 3. Instead of ethanol also other alcohols can be used, such as methanol, ethyleneglycol, or polyvinylalcohol (PVA). In the present work usually a solution of 10^{-3} mol l^{-1} dye **1A** in 10^{-2} mol l^{-1} sodium hydroxide containing 20% ethanol was used to prepare the *J*-aggregates with a double split absorption spectrum. [1]

To perform polarized absorption measurements, a 10^{-6} mol l^{-1} dye solution in 10^{-2} mol l^{-1} sodium hydroxide (in bidistilled water) was mixed one to one with an aqueous PVA solution (5 g PVA, molecular weight 72 000, FLUKA, Buchs, Switzerland, per 150 ml bidistilled water). The

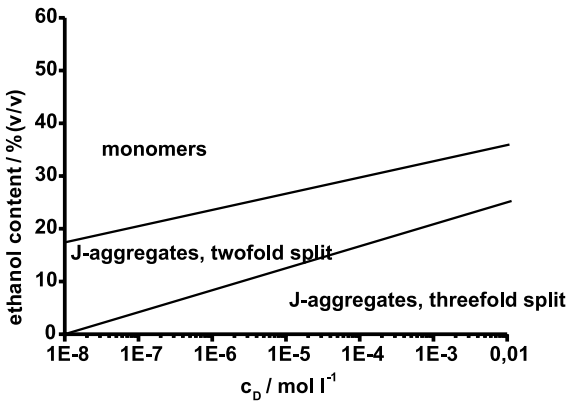

Fig. 3. Regions of existence of monomeric molecules and of *J*-aggregates of dye **1A** with twofold and threefold split *J*-absorption bands solved in 10^{-2} mol l^{-1} aqueous sodium hydroxide solution at room temperature in dependence on dye concentration c_D and on the content of ethanol.

[1] The dye sample **1A** provided by FEW Chemicals [25] consisted of about 50% of the dye bromide shown in Scheme 1 which contains two neutral carboxylic acid substituents R′ and 50% of the dye betaine having two different R′ substituents: $R'_1 = (CH_2)_3COOH$ and $R'_2 = (CH_2)_3COO^-$. Apart from the purification effect through recrystallization of dye **1A** from DMSO, HBr is split off during this procedure, thus producing the pure betaine, which is much better soluble in DMSO than the dye bromide. In Refs. [12–14,18,28] a sample of dye **1A** was used that was contaminated by a certain amount of the precursor from synthesis [26].

spectrum of this mixture, shown in Fig. 4 (solid line), resembles that of the twofold split *J*-aggregates in Fig. 1(a). It possesses a more pronounced absorption in the region of the dye monomers (below 550 nm), the origin of which is not clear yet. As this feature is not polarized (Section 4.2), it seems not to be directly related to extended exciton transitions on the aggregates. Therefore, we ignored it in the further analysis. This solution was then poured onto a planar support and evaporated in the dark. The absorption spectrum of the obtained film kept its twofold split form, with slightly shifted and broadened *J*-peaks, as is shown by the dashed line in Fig. 4. In order to orient the *J*-aggregates, the film was stretched in a hot air stream by a factor of 2.7.

In order to perform fluorescence measurements at low temperature, a glass building solvent containing 20% ethyleneglycol and 80% 10^{-2} moll^{-1} NaOH (in double distilled water) was used to prepare a 10^{-4} moll^{-1} solution of dye **1A**. At room temperature, this solution also reveals a twofold split absorption spectrum, as will be seen in Section 4.2. To prepare a clear glass, a droplet of this solution was placed between two glass slides (0.4 mm thickness each). This sandwich-like sample was then splashed into liquid nitrogen before cooling down by liquid helium evaporation to the aimed temperature. The low-temperature absorption

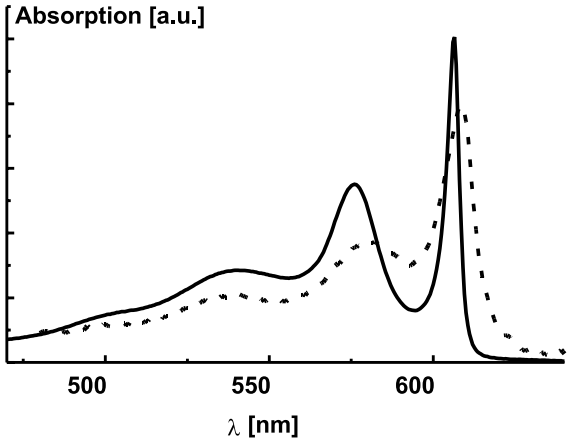

Fig. 4. Absorption spectra of 5×10^{-7} moll^{-1} dye **1A** in 5×10^{-3} moll^{-1} NaOH containing 16.7 gl^{-1} PVA, before (—) and after (- - -) evaporation of the water.

spectrum still reveals the double-peak structure (see Section 4.2). The optical density in the absorption maximum of the prepared samples was about 0.2.

4. Results and discussion

4.1. Absorption spectra

The exciton theory outlined in Section 2 is applied to interpret the spectral behavior of the prepared *J*-aggregates. We first consider the small aggregates with the twofold split absorption band observed in the sodium hydroxide solution (Fig. 1(a)). After deconvolution of the spectrum by asymmetrical Gaussian functions, one finds the transition energies $E_{k=0} = 16\,592$ cm^{-1} and $E_{k=\pm1} = 17\,422$ cm^{-1}, while $E^0 = 19\,000$ cm^{-1} is taken constant for the dye monomers. Substituting these values into Eq. (6) gives $N_{\text{ring}} = 7.3$, implying that the number of molecules within one ring of the cylinder is either 7 or 8. It is also instructive to note that the spectrum reveals the transfer interaction energy $J = (E_{k=0} - E^0)/2 = -1200$ cm^{-1}. This magnitude is typical for *J*-aggregates of cyanine dyes [27] and in fact agrees well with the value obtained for linear TDBC aggregates in solution [34]. Finally, using Eq. (8) and the ratio of the peak areas $A_{k=0}/A_{k=\pm1} = 0.17$ as determined from the spectrum in Fig. 1(a), one obtains a tilt angle of $\beta = 23°$. We point out that the value for angle β is a rather rough estimate, because given the rather large number of fit parameters of each partial peak, the fitting procedure is not free of arbitrariness. In addition it was necessary to take into account some absorption of monomeric dye molecules in the fitting procedure, although no monomers could be detected in the spectra of those dyes **1** whose *J*-aggregates possess only one single *J*-absorption band [e.g. **1**, R = C_2H_5; R′ = $(CH_2)_3SO_3H$] [26]. These uncertainties make it hard to accurately determine the ratio of the peak areas. The ratio may vary between 0.15 and 0.40 and hence, the tilt angles might have values between 20° and 32°.

In order to get an impression of whether these numbers are reasonable, we estimate the diameter of the cylinder that follows from them. Making

such an estimate is not a straightforward problem, as we have little information about the aggregate structure. Taking the molecules to be of rectangular shape of size $L \times H \times D$ (see Fig. 2), one may arrive at the following hand-waving expression for the outer diameter of the cylinder:

$$d = \frac{N_{\text{ring}}}{\pi}(D \sin\beta + L\cos\beta) + 2H. \tag{9}$$

This expression assumes that the side of length H is oriented along the radial direction of each ring and that the molecules are packed as close as their sizes will allow them.[2] Using $N_{\text{ring}} = 7$ (or 8) and $D = 0.4$ nm, $H = 1.0$ nm, $L = 1.9$ nm, as obtained from the van der Waals radii of the molecules [14], we find $d = 6.2$ (or 6.9) nm for $\beta = 23°$. (Owing to the formation of a quasi-liquid phase inside the micellar cylinders [14] the 1.0 nm long octyl side groups have been ignored in this estimate.) It should be emphasized that also the results for d are rather rough, in view of the hand-waving nature of Eq. (9) and the assumption made about the shape of the molecules. Molecular modelling of the cylinders [14] and other estimates, based on somewhat different version of Eq. (9), suggest that $d = 5 \pm 1$ nm. These estimates are not unreasonable as the filtration experiments have shown that the J-aggregates with a twofold split absorption band are smaller in size than the superhelices with threefold split absorption band whose single strands have a diameter of about 10 nm [15].

Although we have hitherto used the cylinder as structural model for the small aggregates, it should be noted that the above results cannot distinguish between single-rings or cylinders built up from (weakly) interacting rings. The polarized absorption measurements of oriented J-aggregates, presented in Section 4.2, however, strongly suggest that the cylinder picture is indeed correct.

We have applied the same analysis to the J-aggregates with twofold J-aggregates that are solved in polymeric PVA solution for preparation the stretched PVA films (Fig. 4, solid line, the peak positions after deconvoluting are: 16 510 cm^{-1} [98.0 cm^{-1}; 11.4], 17 360 cm^{-1} [463.7 cm^{-1}; 26.9], 18 393 cm^{-1} [552.4 cm^{-1}; 9.5] and 19 120 cm^{-1} [1436.0 cm^{-1}; 30.5], $R^2 = 0.9714$, in brackets FWHM and relative areas). As argued in Section 3, we have ignored the second absorption band below 550 nm (at 18 393 cm^{-1}). Doing so, we find $N_{\text{ring}} = 7.6$ from the positions of the two J-bands, in agreement with the value obtained above, while the ratio $A_{k=0}/A_{k=\pm1} = 0.4$ of the two peak areas yields a tilt angle $\beta = 32°$. For the outer diameter of the rings assuming $N_{\text{ring}} = 8$ this gives the value $d = 6.6$ nm.

We now turn to the larger J-aggregates with a threefold split absorption band shown in Fig. 1(b). As explained at the end of Section 2, this spectrum can be understood in a similar way as for the smaller aggregates and our theory can be used to estimate the diameters of the two layers making up the strands that form the superhelices. After deconvoluting the spectrum using asymmetrical Gaussian functions, while the transition energy and band halfwidth of the monomers is taken constant ($E^0 = 19\,000$ cm^{-1}, FWHM = 1436 cm^{-1}), the absorption maxima of the split J-band amount to $E_{k=0} = 16\,636$ cm^{-1}, $E_{k=\pm1} = 17\,199$ cm^{-1} of the middle positioned peak and $E_{k=\pm1} = 17\,861$ cm^{-1} of the other one. It follows from Eq. (6) that the inner ring of the bilayer wall must consist of $N = 6$ molecules and the outer ring of $N = 9$ molecules. We also note that from $E_{k=0}$ and E^0 we obtain $J = -1180$ cm^{-1}, which is almost identical to the interaction obtained for the small J-aggregates with the twofold split band.

In order to estimate the tilt angles β_{in} and β_{out} in both walls, Eq. (8) must be extended to:

$$A_{k=0} = A^{\text{in}}_{k=\pm1}\tan^2\beta_{\text{in}} + A^{\text{out}}_{k=\pm1}\tan^2\beta_{\text{out}}, \tag{10}$$

where $A_{k=0}$ is the total intensity in the lowest J-band, $A^{\text{in}}_{k=\pm1}$ is the total intensity in the highest J-band, and $A^{\text{out}}_{k=\pm1}$ is the total intensity in the middle band. Moreover, the intensity ratio of the middle and lowest bands is given by

$$\frac{A^{\text{in}}_{k=\pm1}}{A^{\text{out}}_{k=\pm1}} = \frac{N_{\text{in}}\cos^2\beta_{\text{in}}}{N_{\text{out}}\cos^2\beta_{\text{out}}}. \tag{11}$$

[2] Although the presumed rectangular shape of the molecules does not permit an optimal intermolecular overlapping, which is necessary for strong coupling, the real overlap might be much better due to an intramolecular twist of the chromophores by 17° around their trimethine chain, like it happens in crystals [19].

Taking the areas of the peaks determined by the deconvolution procedure (cf. legend to Fig. 1(b)), and using $N_{in} = 6$ and $N_{out} = 9$, we arrive at $\beta_{in} = 31°$ and $\beta_{out} = 18°$. As in the case of the twofold split spectrum, these angles are rather rough estimates. It is, in fact, possible that the angles are (almost) identical for both walls. Using Eq. (9), the above numbers translate into an outer diameter of $d = 5.5$ nm for the inner ring, while the outer ring has a diameter of 5.5 nm inside and 7.5 nm outside. The latter value is close to the diameter of 10 nm that was determined for the single strands of the superhelices in the cryo-TEM pictures [15].

4.2. Polarized absorption measurements

By polarized absorption measurements, the polarization of optical transitions of molecules can be determined relative to a given orientation of the sample. For this purpose a homogeneous part of the stretched PVA film of the small *J*-aggregates of dye **1A** having a twofold split *J*-band was vertically fixed in a standard quartz cuvette which could be reproducibly placed into the spectrometer. The spectra were measured with an Omega 2000 absorption spectrometer (Bruins) in single beam modus. In front of the sample a polarizer was fixed, which could be adjusted with an accuracy of 2°. Before measuring the spectra for each position of the polarizer the reference spectrum without any sample was determined. For some selected angles the spectra corrected for this reference, are given in Fig. 5, with the spectra for polarization parallel to and perpendicular to the stretching emphasized by bold lines. The low-energy *J*-band has its maximum value at polarization parallel to the stretching direction and decreases with increasing angle. Simultaneously, the high-energy *J*-band grows and reaches its maximum value perpendicular to the stretching direction. To quantify the amplitudes of the two peaks, the spectrum was deconvoluted using suitable Gaussian absorption profiles. Doing so the amplitude of the low-energy band is found to decrease by a factor of 2.4 when the polarizer is changed from 0° to 90°. Concomitantly, the amplitude of the high-energy band increases by the same factor whereas the absorption below 550 nm exhibits only a weak angle dependence.

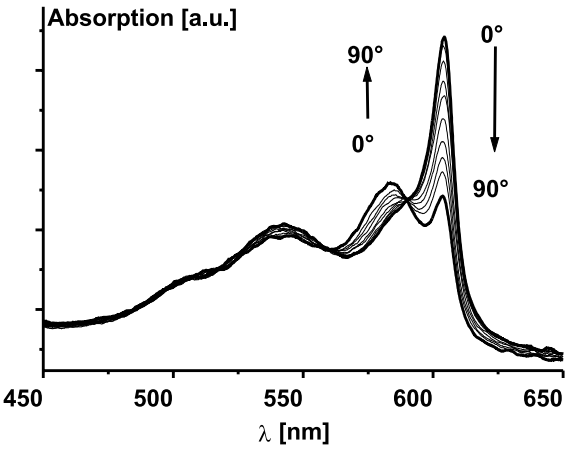

Fig. 5. Absorption spectra of the stretched PVA film containing dye **1A** *J*-aggregates for several polarization angles of the light with respect to the stretching direction. The bold curves emphasize the spectra for polarization parallel (0°) and orthogonal (90°) to the stretching direction, respectively.

This experiment lends strong support to the idea that the smaller *J*-aggregates have a cylindrical structure, similar to the strands that make up the superhelices. Namely, the long axis of a cylinder will orient parallel to the stretching direction, meaning that the low-energy state can indeed be interpreted as the $k = 0$ state, whose transition is polarized parallel to the cylinder axis. If the aggregates would be single rings, one should expect the higher-energy state to be polarized parallel to the film plane, as single rings would tend to orient with their planes inside the stretching direction. Thus, as anticipated already in Section 4.1, we may indeed associate the low-energy *J*-absorption band at 606 nm with the $k = 0$ state of cylindrical aggregates, while the high-energy *J*-band at 576 nm state is associated with the $k = \pm 1$ states.

4.3. Fluorescence polarization

Another way to investigate the polarization of optical transitions is to determine the fluorescence polarization. This is done in isotropic samples by measuring the intensity of the fluorescence with horizontal and vertical polarization (I_h and I_v,

respectively), when exciting the sample with light of vertical polarization and incident right-angled (horizontal) to the detection direction. The fluorescence polarization P is then defined by:

$$P = \frac{I_v - I_h}{I_v + I_h}. \tag{12}$$

Provided that orientational relaxation processes within the fluorescence lifetime do not contribute to the depolarization of the fluorescence, for isotropic samples the maximum fluorescence polarization is $P = 0.5$ in the case that the dipoles of the absorbing and fluorescing transitions are parallel, and $P = -0.33$ in the case that these dipoles are perpendicular to each other.

To avoid reabsorption of the fluorescence, the optical density of the sample was kept smaller than 0.3. This was achieved by using a sample thickness smaller than 0.2 mm and by ensuring a sufficiently high dye concentration for aggregation. The fluorescence was detected in right-angled front face geometry, where the detection angle was about 80° to the surface of the sample. This was done to minimize the influence of the polarization dependent reflection of the fluorescence light at the sample surface. The polarization dependent sensitivity of the detection system, consisting of a double monochromator and photomultiplier, was determined separately by using the isotropically scattered light of a tungsten lamp inside an integrating sphere.

In order to obtain a fluorescence–polarization excitation-spectrum, the dependence of the fluorescence polarization on the excitation wavelength was determined. The results at room temperature are given in Fig. 6, together with the absorption spectrum of the sample. Upon excitation in the region of the $k = 0$ J-band, the fluorescence polarization reaches a positive maximum of $P = 0.31$. At shorter excitation wavelengths, P changes sign and reaches a minimum of $P = -0.23$ in the region of the $k = \pm 1$ J-band. This value is only reached when the emission is detected in its maximum at 610 nm. At longer detection wavelengths, the minimum of the fluorescence polarization is reduced to $P = -0.15$. It is impossible to measure the dependence of P on the detection wavelength within the $k = 0$ J-band, because the scattered excitation light

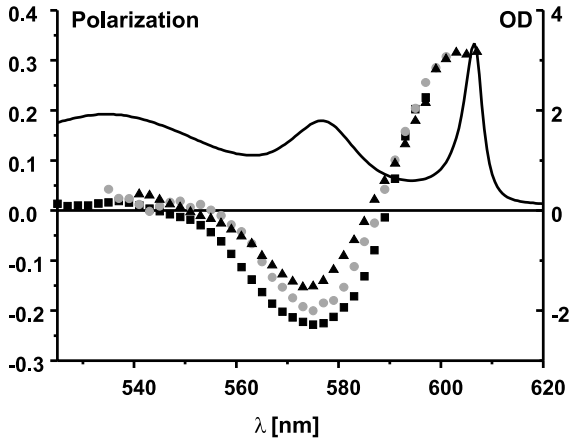

Fig. 6. Room temperature fluorescence polarization (Eq. (12)) measured as a function of excitation wavelength for three different detection wavelengths: (■) 610 nm, (●) 617 nm, (▲) 620 nm. The experiments were done on a solution of 10^{-4} moll^{-1} dye **1A** aggregates in 10^{-2} moll^{-1} NaOH containing 20% ethyleneglycol. The solid curve is the room temperature absorption spectrum of the solution.

prohibits differences smaller than 5 nm between the excitation and the detection wavelengths.

Clearly, these data indicate that, indeed, the absorption and the resonance fluorescence transitions related to the $k = 0$ state are polarized parallel to each other, while the absorption transitions related to the $k = \pm 1$ states are polarized orthogonal to the $k = 0$ state. This is in agreement with the absorption measurements on oriented samples and with the exciton theory of cylindrical J-aggregates explained in Section 2. The dependence of the fluorescence polarization on the emission wavelength probably results from the fact that the lower the energy of the emitting state, the longer the intraband relaxation path towards these states. This enables a more extensive spatial diffusion over the aggregate, which in turn results in a loss of polarization, as we expect that, in analogy to the large aggregates observed in cryo-TEM, the small aggregates are bend with typical radii of several micrometers [15]. This relaxation picture is consistent with the increase in the fluorescence lifetime upon increasing the detection wavelength [28]. Moreover, such spatial diffusion also explains why the observed polarization does not reach the ideal limits of $P = 0.5$ and $P = -0.33$.

We now turn to the low-temperature (4 K) fluorescence depolarization, for which the results are shown in Fig. 7, along with the absorption spectrum at this temperature. The surprising observation is that, while the fluorescence polarization of the $k = 0$ J-band is maintained, the polarization of the $k = \pm 1$ J-band now vanishes. In fact, the polarization near the $k = 0$ J-band approaches with $P = 0.46$ nearly its theoretical maximum. This is the expected behavior, as hardly any thermal reorientation is left at 4 K. By contrast, the behavior near the $k = \pm 1$ J-band is unexpected: the polarization does not change sign and is more or less constant at $P \approx 0.07$. This suggests that at low temperature and upon excitation in the $k = \pm 1$ states, negligible correlation exists between the polarizations of the absorption and fluorescence transitions.

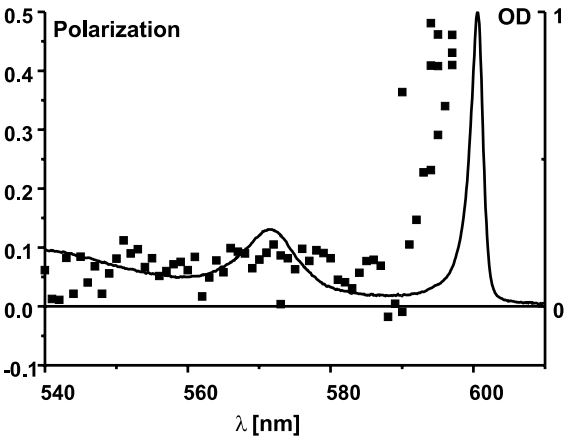

Fig. 7. Low-temperature (4 K) fluorescence polarization (Eq. (12)) measured as a function of excitation wavelength for a detection wavelength of 602 nm. The experiments were done on a cooled solution of 10^{-4} moll^{-1} dye **1A** aggregates in 10^{-2} moll^{-1} NaOH containing 20% ethyleneglycol. The solid curve is the 4 K absorption spectrum.

In order to exclude the possibility that the above observation is an experimental artifact, we made sure that the scattered light of the polarized excitation beam and the polarizing effects of the cryostat windows did not influence the results. To this end, we used a different experimental set-up, in which the fluorescence spectra were measured under identical conditions in such a way that only the wavelength of the vertically polarized excitation light was changed. The results are shown in Fig. 8. When exciting in the $k = 0$ J-band region at 594 nm (Fig. 8(a)) a distinct dependence of the fluorescence intensity on the polarization angle is observed, while for excitation at 573 nm, i.e. in the $k = \pm 1$ J-band (cf. Fig. 8(b)), no polarization of the fluorescence is found. Moreover, the spectra given in Fig. 8(a) show that the fluorescence can be energetically well separated from the scattered excitation light by the monochromator. We also note that the observed surprising behavior is not caused by structural changes in the transparent samples when they are cooled down beyond the glass point of the solvent. Namely, such damage of

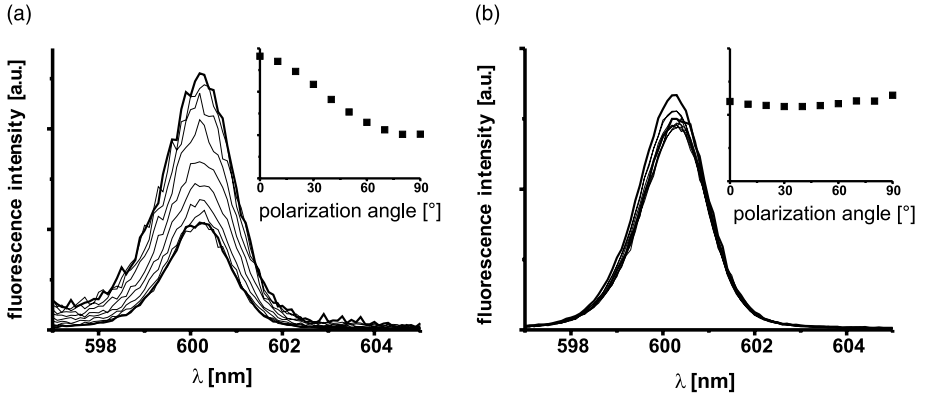

Fig. 8. Corrected emission spectra of the 4 K sample of Fig. 8 for a set of different fluorescence polarization angles. In the two figures all parameters are equal, with the exception of the excitation wavelength: (a) 594 nm; (b) 573 nm. The inserts show the dependence of the integral fluorescence intensity on the polarization angle.

the glassy matrix should equally influence the fluorescence polarization in the $k = \pm 1$ and the $k = 0$ J-bands.

We have been unable to pinpoint with certainty the origin of the surprising low-temperature depolarization behavior. In the following, we discuss several possibilities, which all need further research. We first note that, as reorientation of the J-aggregates within the experimental time scale is impossible at 4 K, it appears that any loss of polarization should be related to spatial migration of the excitation. This may take place either within one aggregate or between different aggregates. As the aggregates might be bended on the micrometer scale (see above) and cross-linked aggregates do not have the same orientation, this indeed leads to the loss of polarization. While extensive exciton diffusion at low temperature seems to be excluded on theoretical grounds [29], it should be noted that recent exciton–exciton annihilation experiments in THIATS J-aggregates have shown a surprisingly strong low-temperature annihilation efficiency [30]. One contributing factor in spatial sampling possibilities of the excitation, is the fact that at low temperature the excitons have a larger coherence length than at room temperature [31–34], because the effect of phonon scattering is eliminated. At low temperature, this length scale is limited only by the exciton delocalization length imposed by static disorder. It seems, though, that this would equally affect the depolarizing behavior of the $k = \pm 1$ states and the $k = 0$ state, which contradicts our experiments. It should be noted, however, that the delocalization length of the $k = \pm 1$ states may be enhanced compared to the $k = 0$ state, due to the fact that they arise from two (almost) degenerate states with mutually perpendicular polarization. Such an effect was recently observed in model calculations on discotic aggregates [35]. We also note that in general an efficient transport of the $k = 0$ excitation energy from one aggregate to another is only possible when the aggregates cross each other in an almost parallel way. For larger crossing angles, the dipoles of the $k = \pm 1$ states give more possibility to transfer energy.

Finally, it should be noted that the anomalous depolarizing behavior may have an entirely different origin, which resides in the appreciable amount of energy ($\sim$1000 cm^{-1}) that has to be dumped into the environment when nonradiatively relaxing from the excited $k = \pm 1$ states to the emitting $k = 0$ state. In the low-temperature glass, this may give rise to local heating, enabling further diffusion, or even local configuration changes or fracture of the glass. The latter may lead to reorientation of the aggregate and (or) scattering of the emission light, which both contribute to polarization loss. A similar heating effect does not occur upon excitation in the $k = 0$ band, because then it is not necessary to dump a similar amount of energy before the emission process takes place.

5. Conclusions

Using polarized absorption and fluorescence depolarization experiments, we have found strong indication that the small chiral J-aggregates of dye **1A** with the twofold split absorption band, have a cylindrical structure, similar to the single strands of the large superhelices observed in cryo-TEM, which exhibit a threefold split J-band. From the absorption spectra, we were able to extract estimates for the diameters of the cylinders, both for the twofold and the threefold split case. These estimates are in rough agreement with the TEM pictures. The cylinders of the superhelices probably have bilayer walls, while the cylinders of the small J-aggregates seem to have a single-walled micellar structure. The small J-aggregates demonstrate surprising low-temperature depolarization dynamics, which is either related to preferential exciton migration or to a local heating effect arising from energy released in nonradiative relaxation preceding the spontaneous emission process.

Throughout this paper, we have restricted ourselves to nearest-neighbor interactions between molecules within the rings that make up the cylinders. Longer-range interactions and interactions between different rings have been neglected in the analysis. We stress that including additional interactions does not lead to major changes in the basic picture: three dipole allowed transitions dominate the absorption spectrum. One of these is

polarized along the cylinder axis, while the other two are degenerate and polarized perpendicular to the axis. This statement is rigorous if we assume periodic boundary conditions in the longitudinal direction of the cylinder (i.e., if the cylinder is long), as in that case the states are two-dimensional Bloch states with optical selection rules imposing a zero wave number for the longitudinal direction and $k = 0$ or $k = \pm 1$ for the circumferential direction. These selection rules do not depend on the range of the interaction, but only rely on the Bloch nature and the geometry of the transition dipoles on the cylinder [21]. For open boundary conditions in the longitudinal cylinder direction, the situation changes and, in principle, more transitions obtain oscillator strength. Yet, for the assumed cylinder geometry, each one of these transitions is either polarized along the cylinder axis, or perpendicular to it (independent of the interactions and the tilt angle β). Moreover, in analogy to one-dimensional *J*-aggregates with nearest-neighbor [36] as well as with long-range dipole interactions [37], one expects that only one superradiant longitudinal wave function dominates the optical absorption [24]. Thus, the basic picture of three dominant transitions (one polarized along the cylinder axis and two perpendicular to it) is not changed by including additional interactions. To illustrate possible effects, we note that the absorption experiments reported here, have also been analyzed using a model in which dipole-dipole interactions are used between neighboring molecules within rings, between neighboring molecules on adjacent rings, as well as between the nearest-neighbor molecules in the diagonal directions of the underlying lattice [21]. This model leads to a circumference of 7.8 instead of 7.3 molecules and an interaction in the ring direction that is decreased by roughly 15% relative to the value of -1200 cm^{-1} which we found in Section 4.1.

We finally note that micellar molecular tubes are also found in nature, where they occur as light-harvesting systems: strong evidence exists that the chlorosomes of green bacteria consist of a well-defined tubular arrangement of many ($\sim 10^2$) bacteriochlorophyll molecules [38]. We believe that the amphi-PIPEs which we reported on above are promising candidates for artificial light-harvesting systems, to be used in photoinduced electron transfer reactions, because they combine the self-assembling ability of amphiphilic molecules to form cyclic structural units, with the unique features of *J*-aggregates for energy migration over long distances. However, further investigations, such as time-dependent fluorescence, pump–probe, and exciton–exciton annihilation experiments will have to be done in order to further clarify the exciton migration processes in these cylindrical *J*-aggregates.

Acknowledgements

We highly appreciate the promoting part played by Prof. Dr. Friedrich Doerr, Munich, in the field of *J*-aggregation phenomena on occasion of his 80th birthday. We are also very grateful to Prof. Dr. Hans Kuhn who gave us valuable hints in preparing suitable polymeric films and informed us about his helix model of dye **1A** based on the extended dipole model [27] in good time. We acknowledge helpful discussions with Mrs. Stephania Lampoura. This work was supported by the Deutsche Forschungsgemeinschaft (SFB 337, AB 74/5-3). Travel support enabling crucial discussions was obtained from INTAS (project 97-10434).

References

[1] G. McDermott, S.M. Prince, A.A. Freer, A.M. Hawthornthwaite-Lawless, M.Z. Papiz, R.J. Cogdell, N.W. Isaacs, Nature 374 (1995) 517.
[2] W. Kuehlbrandt, D.N. Wang, Y. Fujiyoshi, Nature 367 (1994) 614.
[3] X. Hu, K. Schulten, Phys. Today 50 (8) (1997) 28;
H. van Amerongen, L. Valkunas, R. van Grondelle, Photosynthetic Excitons, World Scientific, Singapore, 2000.
[4] See, e.g., M.V. Mostovoy, J. Knoester, J. Phys. Chem. B 104 (2000) 12355, and references therein.
[5] A.M. van Oijen, M. Ketelaars, J. Köhler, T.J. Aartsma, J. Schmidt, Science 285 (1999) 400.
[6] G. Scheibe, A. Schoentag, F. Katheder, Naturwissenschaften 29 (1939) 499.
[7] S. Daehne, U. De Rossi, J. Moll, J. Soc. Phot. Sci. Technol. Japan 59 (1996) 250.
[8] E.G. McRae, M. Kasha, J. Chem. Phys. 28 (1958) 721.

[9] M. Kasha, in: L. Augenstein, R. Mason, B. Rosenberg (Eds.), Spectroscopy of the Excited State, Academic Press, New York, 1964, p. 23.
[10] E.W. Knapp, Chem. Phys. 85 (1984) 73.
[11] J. Knoester, J. Chem. Phys. 99 (1993) 8466.
[12] U. De Rossi, J. Moll, M. Spieles, G. Bach, S. Daehne, J. Kriwanek, M. Lisk, J. Prakt. Chem. 337 (1995) 203.
[13] U. De Rossi, S. Daehne, S.C.J. Meskers, H.P.J.M. Deckers, Angew. Chem. 108 (1996) 827;
U. De Rossi, S. Daehne, S.C.J. Meskers, H.P.J.M. Deckers, Angew. Chem. Int. Ed. Engl. 35 (1996) 760.
[14] A. Pawlik, S. Kirstein, U. De Rossi, S. Daehne, J. Phys. Chem. B 101 (1997) 5646.
[15] H. von Berlepsch, C. Boettcher, A. Ouart, C. Burger, S. Daehne, S. Kirstein, J. Phys. Chem. B 104 (2000) 5255.
[16] H. von Berlepsch, C. Boettcher, A. Ouart, M. Regenbrecht, S. Akari, U. Keiderling, H. Schnablegger, S. Daehne, S. Kirstein, Langmuir 16 (2000) 5908.
[17] C. Spitz, S. Daehne, A. Ouart, H.-W. Abraham, J. Phys. Chem. B 104 (2000) 8664.
[18] C. Spitz, S. Daehne, Ber. Bunsenges. Phys. Chem. 102 (1998) 738.
[19] S. Kirstein, H. von Berlepsch, C. Boettcher, C. Burger, A. Ouart, G. Reck, S. Daehne, CHEMPHYSCHEM (2000) 146.
[20] A.S. Davydov, Theory of Molecular Excitons, Plenum Press, New York, 1971.
[21] M. Bednarz, J. Knoester, J. Phys. Chem. B, in press.
[22] V.I. Novoderezhkin, A.P. Razjivin, Biophys. J. 68 (1995) 1089.
[23] L.D. Bakalis, M. Coca, J. Knoester, J. Chem. Phys. 110 (1999) 2208.
[24] C. Didraga, J. Knoester, Chem. Phys. 275 (2002) 307–318.
[25] FEW Chemicals, Forschungs- und Entwicklungsgesellschaft Wolfen mbH, Industriepark Wolfen-Thalheim, Postfach 1340, D-06756 Wolfen.
[26] A. Ouart, Ph.D. Thesis, Humboldt-Universitaet, Berlin, 2000. http://dochost.rz.hu-berlin.de/dissertationen/ouart-andre-2000-09-28/PDF/Ouart.pdf.
[27] H. Kuhn, C. Kuhn, in: T. Kobayashi (Ed.), J-aggregates, World Scientific, Singapore, 1996.
[28] C. Spitz, Ph.D. Thesis, Free University of Berlin, 1999. http://www.diss.fu-berlin/1999/15.
[29] I.V. Ryzhov, G.G. Kozlov, V.A. Malyshev, J. Knoester, J. Chem. Phys. 114 (2001) 5322.
[30] I.G. Scheblykin, O.Y. Sliusarenko, L.S. Lepnev, A. Vitukhnovsky, M. Van der Auweraer, J. Phys. Chem. B 104 (2000) 10949.
[31] H. Fidder, D.A. Wiersma, J. Phys. Chem. 97 (1993) 11603.
[32] J.R. Durrant, J. Knoester, D.A. Wiersma, Chem. Phys. Lett. 222 (1994) 450.
[33] J. Moll, S. Daehne, J.R. Durrant, D.A. Wiersma, J. Chem. Phys. 102 (1995) 6362.
[34] M. van Burgel, D.A. Wiersma, K. Duppen, J. Chem. Phys. 102 (1995) 20.
[35] D. Markovitsi, L.K. Gallos, J.P. Lemaistre, P. Argyrakis, Chem. Phys. 269 (2001) 147.
[36] H. Fidder, J. Knoester, D.A. Wiesma, J. Chem. Phys. 95 (1991) 7880.
[37] V.A. Malyshev, P. Moreno, Phys. Rev. B 51 (1995) 14587.
[38] V.I. Prokhorenko, D.B. Steensgaard, A.R. Holzwarth, Biophys. J. 79 (2000) 2105.